Reactions of Group 3 Transition Metal Atoms with CS_2 and OCS: Matrix Isolation Infrared Spectra and Density-Functional Calculations of SMCS, SM-(η^2-CS), SMCO, and SM-(η^2-CO) in Solid Argon

Alexander B. Baker and Lester Andrews*

Department of Chemistry, University of Virginia, P.O. Box 400319, Charlottesville, Virginia 22904-4319

Received: May 19, 2006; In Final Form: July 13, 2006

Laser-ablated scandium, yttrium, and lanthanum atoms were reacted with CS_2 and OCS molecules in an argon matrix. Products of the type SMCX and S−M(η^2-CX) (X = S or O) were formed on sample deposition. Photolysis favored the S−M(η^2-CX) complex, while annealing increased the more stable SMCX isomer. Product absorptions are identified by density-functional frequency calculations and isotopic substitutions. This work reports the first vibrational spectroscopic characterization of Sc, Y, and La reaction products with CS_2 and OCS and the subsequent interconversion between SMCX and S−M(η^2-CX) structural isomers.

Introduction

Transition metal complexes play an important chemical role in biological and catalytic systems. Interactions between CO_2 and transition metals have been of interest for many years.[1] For example, transition metals enable anaerobic CO_2 fixation by enzymes, converting CO_2 to methane using iron, nickel, and copper contained in the active site.[2] Extensive experimental and theoretical studies of transition metal−CO_2 complexes have been reported.[3−13] Molecular beam experiments have been conducted with CO_2 and vanadium ions to examine energy-dependent photochemistry.[14] Carbon monoxide bond cleavage by titanium atoms has been studied theoretically.[15] Reaction products of the type OMCS, $OMCO^+$, $OMOC^+$, OM−(η^2-CO), and $O_2M(CO)_2$ have been identified by matrix IR spectroscopy.[16−18] Additionally, binding energies of the gaseous complexes M^+−CO_2 have been described, providing additional comparative data.[14,19,20]

However, transition metal reactions with CS_2 have received less attention. Only a few theoretical[21−23] and experimental[24−31] studies have been performed to date, mostly involving gas-phase reactions with metal cations. Isovalent with CO_2, CS_2 is used similarly in both organic and organometallic reactions.[1] Given such a broad interest in CO_2, a more detailed understanding of reactions between transition metals and CS_2 is warranted. Moreover, there is current interest in transition metal sulfides due to applications in catalysis and electronics.[32] An additional comparison can also be drawn from carbonyl sulfide (OCS). To our knowledge, OCS has not been reacted with transition metal atoms. In this paper, we report a study of laser-ablated Sc, Y, and La atom reactions with CS_2 and OCS in solid argon. We will show evidence supporting the formation of S−M−CS and SM(η^2-CS) products with CS_2 and their photochemical interconversion. In a sense, this is similar to the photochemical reversibility of the analogous S_4 isomers.[33,34] With OCS, evidence is found for only CS insertion products (S−M−CO and SM(η^2-CO)).

Experimental and Computational Methods

The experimental methods for laser ablation and matrix isolation have been previously reported.[35−37] Metal atoms were ablated from a rotating metal target using a Nd:YAG laser (1064 nm) with 1−5 mJ/pulse. Reactant molecules in excess argon were co-deposited with the ablated metal atoms onto an 8 K CsI window at 2−4 mmol/h for 30 min. CS_2 (Mallinckrodt), $^{13}C^{32}S_2$ (Cambridge Isotopes), $^{12}C^{34}S_2$ (Oak Ridge National Laboratory), and OCS (Matheson) were employed in different experiments. The natural isotopic OCS sample was purified through several freeze−pump−thaw cycles with liquid N_2. Due to CO_2 impurity in the OCS sample, the first third of the sample was discarded and the sample was prepared with the middle third distilled from glass beads. IR spectra were recorded using a Nicolet Magna 550 spectrometer at 0.5 cm^{-1} resolution and with an accuracy of 0.1 cm^{-1}, using a HgCdTe detector cooled to 77 K. A medium-pressure mercury arc lamp (outer globe removed) coupled with various optical filters was used for sample irradiation followed by annealing in sequence for the same matrix sample.

Electronic structure calculations were done to support the identity of product molecules. The Gaussian 98 program[38] was used with density-functional theory methods (B3LYP[39,40] and BPW91[41,42]). For basis sets, 6-311+(2d) for nonmetals[43,44] and an SDD pseudopotential for metals[45] were used for all calculations. Frequencies were computed analytically and energies include zero-point corrections. Geometries were fully optimized.

Results

Infrared Spectra. IR spectra were recorded for laser-ablated scandium, yttrium, and lanthanum co-deposited with CS_2 in argon. Product absorptions are listed in Tables 1−3, and representative spectra are shown in Figures 1−3. Diatomic CS absorptions, which have been previously reported,[46] are marked for comparison when appropriate. Reactions with trace O_2 impurity produced MO molecules, which have been previously reported.[47,48] Isotopic experiments were performed for mode identification. IR spectra were also recorded for laser-ablated group 3 metals co-deposited with OCS in argon. Weak CO_2 reaction products were observed from impurity in the OCS sample.[17] Product absorptions are reported in Table 4. Figure 4 contains representative spectra for each of the transition metals with photolysis and annealing behaviors.

* To whom correspondence should be addressed. E-mail: lsa@virginia.edu.

10.1021/jp063090o CCC: $33.50
Published on Web 08/15/2006

TABLE 1: Observed Frequencies and Frequencies and Intensities Calculated at Different Levels of Theory for the S−Sc−C═S and S−Sc−(η^2-C═S) Products in the Sc + CS_2 Reaction[a]

	S−Sc−C═S					^{34}S−Sc−C═^{34}S			S−Sc−^{13}C═S		
approx mode	obs	calc[b]	int	calc[c]	int	obs	calc[b]	int	obs	calc[b]	int
C═S stretch	1270.8	1274.8	158	1229.3	207	1263.4	1268.3	156	1232.2	1237.2	152
Sc−S stretch	535.2	551.5	126	528.7	61	525.9	541.4	119	535.1	550.7	122
Sc−C stretch		372.0	41	377.2	26		366.0	40		368.0	40
S−C−Sc bend		213.4	3	228.2	2		215.1	3		209.4	3
S−C−Sc bend o.p.		162.4	31	169.9	30		164.6	31		159.6	29
S−Sc−C═S distort		56.9	11	50.9	12		56.7	11		58.0	11

	S−Sc−(η^2−C═S)					^{34}S−Sc−(η^2−C═^{34}S)			S−Sc−(η^2−^{13}C═S)		
approx mode	obs	calc[b]	int	calc[c]	int	obs	calc[b]	int	obs	calc[b]	int
C═S stretch	1042.3/1035.4/1027.7	1035.7	65	1007.9	72	1034.0	1027.0	64	1013.3/1006.6/999.1	1006.7	63
Sc−S stretch	544.6/539.0	556.2	116	532.7	62	535.2/530.0	547.0	115	544.1/538.7	556.1	115
Sc−C stretch		452.1	40	450.8	25		451.7	38		438.8	39
S−C−Sc bend		230.7	12	225.6	10		227.0	12		229.6	12
S−Sc−C bend		112.1	10	104.7	6		111.5	10		109.3	10
S−Sc−C═S distort		79.6	10	81.8	8		77.8	9		79.6	10

[a] Frequencies and intensities are in cm^{-1} and km/mol. Intensities are all calculated values. [b] B3LYP/6-311+G(2d)/SDD. [c] BPW91/6-311+G(2d)/SDD.

TABLE 2: Observed Frequencies and Frequencies and Intensities Calculated at Different Levels of Theory for the S−Y−C═S and S−Y(η^2-C═S) Products in the Y + CS_2 Reaction[a]

	S−Y−C═S					^{34}S−Y−C═^{34}S			S−Y−^{13}C═S		
approx mode	obs	calc[b]	int	calc[c]	int	obs	calc[b]	int	obs	calc[b]	int
C═S stretch	1231.6/1227.4/1224.0 1199.3/1190.2/1186.4	1259.2	119	1214.7	165	1223.8/1219.6/1216.6 1193.4/1183.8/1180.3	1251.2	115	1194.2/1188.8/1185.7 1161.5/1152.5/1148.9	1220.8	114
Y−S stretch	468.0	469.8	83	456.6	56	458.2	459.6	80	468.0	469.8	83
Y−C stretch		314.9	35	319.0	21		310.9	35		311.8	35
S−C−Y bend		213.0	4	216.0	3		211.6	4		206.8	3
S−C−Y bend o.p.		164.2	28	163.9	28		163.7	28		158.7	26
S−Y−C═S distort		59.0	10	52.1	9		57.6	10		59.0	10

	S−Y−(η^2-C═S)					^{34}S−Y−(η^2-C═^{34}S)			S−Y−(η^2-^{13}C═S)		
approx mode	obs	calc[b]	int	calc[c]	int	obs	calc[b]	int	obs	calc[b]	int
C═S stretch	1038.0	1029.7	55	999.2	69	1029.6	1021.1	53	1008.9	1000.8	53
Y−S stretch	468.0	469.6	76	457.3	46	458.2	459.3	73	468.0	469.5	76
Y−C stretch		405.5	44	403.4	26		405.5	43		391.9	41
S−C−Y bend		201.5	10	200.9	8		197.6	10		200.7	10
S−Y−C bend		111.4	6	110.1	4		110.7	6		108.3	6
S−Y−C═S distort		73.1	8	74.4	7		71.4	8		73.1	8

[a] Frequencies and intensities are in cm^{-1} and km/mol. Intensities are all calculated values. [b] B3LYP/6-311+G(2d)/SDD. [c] BPW91/6-311+G(2d)/SDD.

Calculations. A previous study of late transition metals with CS_2 reported calculations on MCS_2 isomers of the following types: SMCS, SM(η^2-CS), M(η^2-CS)S, and M(η^2-S_2)C.[26] With OCS, we performed calculations for the major products of the CS_2 calculations (SMCO, OMCS, SM(η^2-CO), and OM(η^2-CS)), taking into account the possibility of either CS or CO insertion. In the case of both CS_2 and OCS reactions, the doublet spin state product was lower in energy than the quartet state by between 15 and 30 kcal/mol. These are well-defined doublet ground states with $\langle s^2 \rangle$ values in the 0.750−0.756 range. Our calculated vibrational frequencies and intensities for observed products appear in Tables 1−4 with the corresponding experimental values. B3LYP and BPW91 functional results with the same basis set were presented for all reactions, whereas B3LYP alone is shown for isotopic frequencies to avoid confusion. For Sc, Y, and La, the SMCS product was calculated to be the most stable, followed by the SM(η^2-CS) product (about 10 kcal/mol less stable).

For the CS_2 reactions, the relative B3LYP energies with respect to reactants for S−Sc−CS, S−Y−CS, and S−La−CS were −40, −48, and −57 kcal/mol, respectively. With BPW91, these were −56, −67, and −83 kcal/mol, respectively. B3LYP energies of S−Sc(η^2-CS), S−Y(η^2-CS), and S−La(η^2-CS) were −38, −46, and −55 kcal/mol, respectively. With BPW91, these were −52, −65, and −80 kcal/mol, respectively. Additional possible products were also calculated. The relative energies of the M(η^2-CS)S product were approximately 25 kcal/mol higher on average. However, the predicted frequencies for these molecules were not observed. In addition, B3LYP predicted that the simple M(η^2-S_2)C adduct would be less stable than the SMCS product by only 1 kcal/mol. However, BPW91 predicted slightly (1 kcal/mol) increased stability for this product. In any case, the calculated frequencies with significant IR intensity for M(η^2-S_2)C are below our frequency limit of detection. Relative B3LYP energies are given in Figure 5 along with calculated structures for the S−M−CS and S−M(η^2-CS) products.

Computations on group 3 reaction products with OCS revealed that doublet SMCO and doublet SM(η^2-CO) complexes were the most stable. For example, with B3LYP, the SMCO product for Sc, Y, and La was found to be −48, −55, and −67 kcal/mol more stable than reactants, respectively. The SM(η^2-CO) adducts were less stable with B3LYP energies of −41, −49, and −59 kcal/mol, respectively. As described previously,[49] CS insertion was found to be more favorable than CO insertion.

TABLE 3: Observed Frequencies and Frequencies and Intensities Calculated at Different Levels of Theory for the S−La−C═S and S−La−(η^2-C═S) Products in the La + CS_2 Reaction[a]

	S−La−C═S					^{34}S−La−C═^{34}S			S−La−^{13}C═S		
approx mode	obs	calc[b]	int	calc[c]	int	obs	calc[b]	int	obs	calc[b]	int
C═S stretch	1206.4	1234.9	218	1196.7	233	1200.2	1226.6	213	1168.0	1197.7	208
La−S stretch	428.0	420.7	84	413.9	58	418.0	410.6	81	428.0	420.6	84
La−C stretch		268.1	21	270.4	12		264.6	20		264.5	21
S−C−La bend		195.9	5	198.9	4		194.4	5		190.3	4
S−C−La bend o.p.		156.8	30	159.2	29		156.3	30		151.4	28
S−La−C═S distort		52.1	8	40.2	7		50.8	7		52.0	8
	S−La−(η^2-C═S)					^{34}S−La−(η^2-C═^{34}S)			S−La−(η^2-^{13}C═S)		
approx mode	obs	calc[b]	int	calc[c]	int	obs	calc[b]	int	obs	calc[b]	int
C═S stretch	1044.6	1049.8	86	1021.7	87	1036.7	1041.2	83	1015.6	1020.3	82
La−S stretch	428.0	425.5	73	418.1	52	418.0	415.3	69	428.0	425.3	75
La−C stretch		353.3	43	353.0	26		353.2	43		341.0	39
S−C−La bend		166.7	7	166.7	6		163.1	7		166.0	7
S−La−C bend		117.8	5	113.9	4		117.2	5		114.3	4
S−La−C═S distort		68.3	6	70.2	5		66.6	6		68.3	6

[a] Frequencies and intensities are in cm^{-1} and km/mol. Intensities are all calculated values. [b] B3LYP/6-311+G(2d)/SDD. [c] BPW91/6-311+G(2d)/SDD.

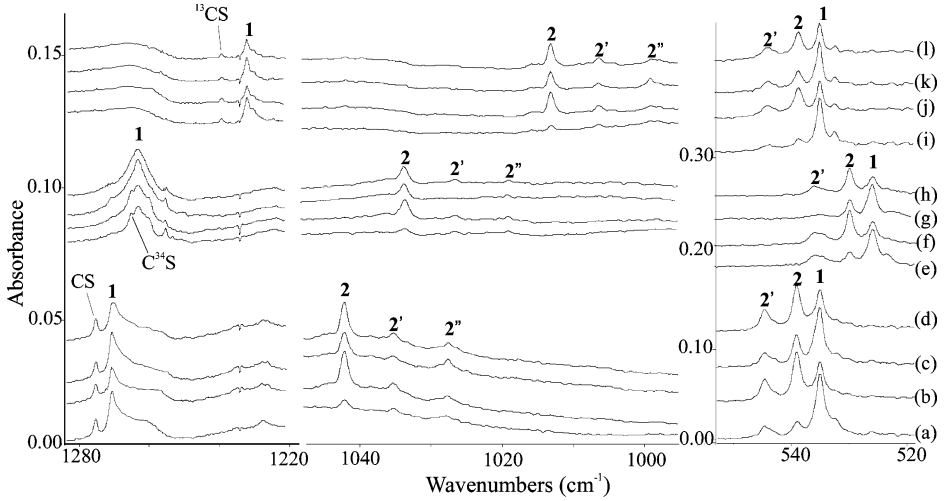

Figure 1. IR spectra in the 1280−1220, 1040−1000, and 550−520 cm^{-1} regions for Sc and CS_2: (a) after 30 min ablation of Sc with 0.5% $^{12}C^{32}S_2$ co-deposited in argon at 8 K, (b) after 10 min of mercury arc lamp irradiation $\lambda > 290$ nm, (c) after annealing to 25 K, and (d) after 10 min broadband ($\lambda > 220$ nm) irradiation; (e) deposition of Sc + $^{12}C^{34}S_2$, (f) $\lambda > 290$ nm irradiation, (g) annealing to 25 K, and (h) broadband irradiation; (i) deposition of Sc + $^{13}C^{32}S_2$, (j) $\lambda > 290$ nm irradiation, (k) annealing to 25 K, and (l) broadband irradiation. Labels 1 and 2 refer to the SScCS and SSc(η^2-CS) products, respectively. Primes differentiate matrix sites.

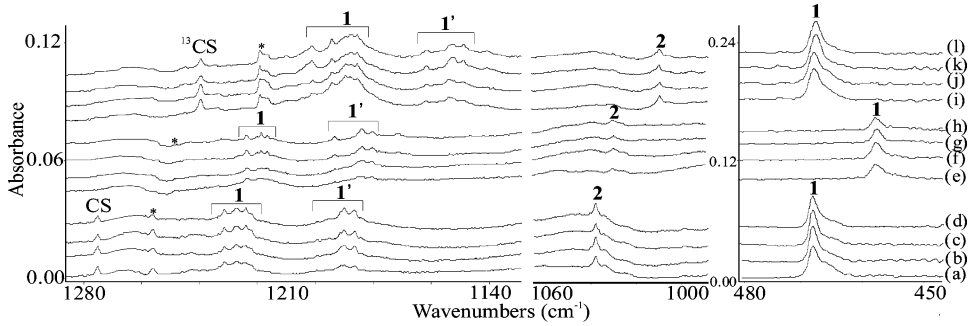

Figure 2. IR spectra in the 1280−1140, 1060−1000, and 480−450 cm^{-1} regions for Y + CS_2: (a) after 30 min ablation of Y with 0.5% $^{12}C^{32}S_2$ co-deposited in argon at 8 K, (b) after 10 min of mercury arc lamp irradiation $\lambda > 290$ nm, (c) after annealing to 25 K, and (d) after 10 min broadband ($\lambda > 220$ nm) irradiation; (e) deposition of Y + $^{12}C^{34}S_2$, (f) $\lambda > 290$ nm irradiation, (g) annealing to 25 K, and (h) broadband irradiation; (i) deposition of Y + $^{13}C^{32}S_2$, (j) $\lambda > 290$ nm irradiation, (k) annealing to 25 K, and (l) broadband irradiation. Labels 1 and 2 refer to the SYCS and SY(η^2-CS) products, respectively. Primes differentiate matrix sites. Asterisks are used to denote impurity.

OMCS energies with B3LYP were −41, −27, and −34 kcal/mol for Sc, Y, and La, respectively. The OM(η^2-CS) isomers were less stable with B3LYP energies of −24, −25, and 18 kcal/mol for Sc, Y, and La, respectively. The high energy O−Sc−CS and O−La−(η^2-CS) species are not explored here, as neither product is seen in the spectra for any of the group 3 metals. Relative B3LYP energies and calculated structures for the S−M−CO and S−M(η^2-CO) products are given in Figure 6.

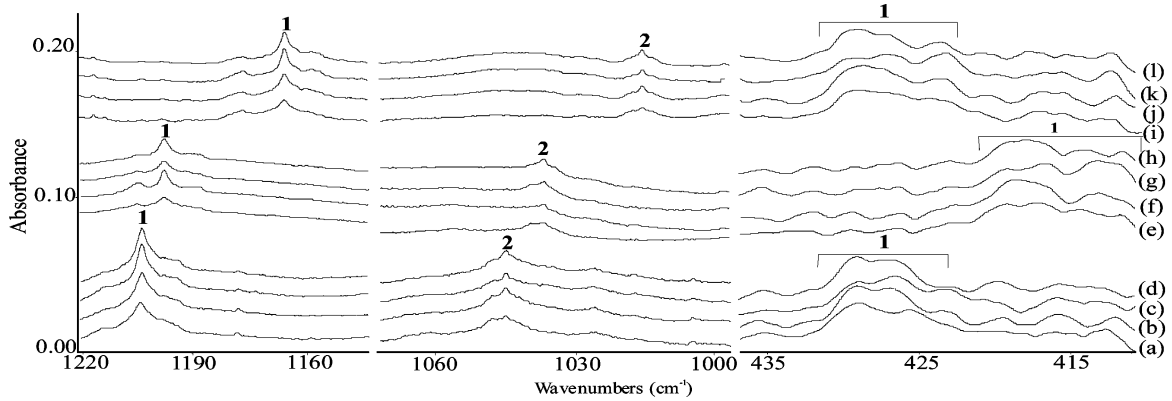

Figure 3. IR spectra in the 1220−1140, 1060−1000, and 430−400 cm^{-1} regions for La and CS_2: (a) after 30 min ablation of La with 0.5% $^{12}C^{32}S_2$ co-deposited in argon at 8 K, (b) after 10 min of mercury arc lamp irradiation $\lambda > 290$ nm, (c) after annealing to 25 K, and (d) after 10 min broadband ($\lambda > 220$ nm) irradiation; (e) deposition of La + $^{12}C^{34}S_2$, (f) $\lambda > 290$ nm irradiation, (g) annealing to 25 K, and (h) broadband irradiation; (i) deposition of La + $^{13}C^{32}S_2$, (j) $\lambda > 290$ nm irradiation, (k) annealing to 25 K, and (l) broadband irradiation. Labels 1 and 2 refer to the SLaCS and SLa(η^2-CS) products, respectively.

TABLE 4: Observed Frequencies and Frequencies and Intensities Calculated at Different Levels of Theory for the S−M−C═O and S−M−(η^2-C═O) Products in the Group 3 Metal Atom and OCS Reactions[a]

	S−Sc−C═O					S−Y−C═O					S−La−C═O				
approx mode	obs	calc[b]	int	calc[c]	int	obs	calc[b]	int	calc[c]	int	obs	calc[b]	int	calc[c]	int
C═S stretch	1898.4	2004.4	1149	1925.9	796	1884.0	1977.7	1018	2001.3	590	1879.0	1984.3	1435	1918.0	1022
M−S stretch		539.9	103	527.2	61		468.2	76	461.6	33		421.0	78	416.0	58
M−C stretch		398.6	1	414.5	2		350.5	3	410.9	22		285.4	0	296.3	0
M−C═O bend		299.8	1	321.9	0		282.1	1	254.3	8		249.3	0	256.4	1
M−C═O bend o.p.		256.4	6	258.2	8		219.9	0	242.5	6		243.2	16	239.9	17
S−M−C distort		59.7	9	65.5	9		61.6	7	120.9	30		56.8	5	44.1	5
	S−Sc(η^2-C═O)					S−Y(η^2-C═O)					S−La(η^2-C═O)				
approx mode	obs	calc[b]	int	calc[c]	int	obs	calc[b]	int	calc[c]	int	obs	calc[b]	int	calc[c]	int
C═S stretch	1617.9	1697.7	379	1656.1	257	1611.8	1681.1	428	1639.1	374	1601.8	1741.1	705	1693.1	477
M−S stretch	544	559.9	109	545.0	79	471.3	474.4	77	468.0	61		427.3	82	422.7	66
M−C stretch		360.5	5	361.3	7		328.6	14	319.9	8		285.7	8	280.3	5
M−C═O bend		344.6	13	317.5	10		309.7	4	286.6	5		243.2	3	234.5	4
M−C═O bend o.p.		140.6	4	140.5	3		138.1	2	137.0	2		144.4	1	141.6	1
S−M−C distort		101.0	11	97.5	9		90.1	9	91.8	6		81.7	6	82.7	5

[a] Frequencies and intensities are in cm^{-1} and km/mol. Intensities are all calculated values. [b] B3LYP/6-311+G(2d)/SDD. [c] BPW91/6-311+G(2d)/SDD.

Discussion

By examining scandium, yttrium, and lanthanum experiments separately, S−M−CS, S−M(η^2-CS), S−M−CO, and S−M(η^2-CO) products will be identified.

Sc + CS_2. A new absorption was observed at 1270.8 cm^{-1} in scandium experiments, which decreased during visible (not shown in Figure 1) and ultraviolet photolysis in sequence on the same sample but increased upon annealing. This band shifted to 1263.0 cm^{-1} with $^{12}C^{34}S_2$ and to 1232.2 cm^{-1} with $^{13}C^{32}S_2$. The isotopic 12-32/13-32 frequency ratio of 1.0313 and 12-32/12-34 ratio of 1.0062 and band position suggest a C═S stretching mode, as similar ratios (1.0291, 1.0081) have been observed for the 1275.1 cm^{-1} CS absorption.[46] However, note the increase in carbon and decrease in sulfur character for this normal mode. A second set of product absorptions was observed in the region around 1050 cm^{-1}. Specifically, bands at 1042.3, 1035.4, and 1027.7 cm^{-1} with CS_2 shifted to 1013.3, 1006.6, and 999.1 with $^{13}C^{32}S_2$. With $^{12}C^{34}S_2$, the satellite peaks were weaker as we observed consistently weaker absorptions for $^{12}C^{34}S_2$ products. The 12-32/13-32 frequency ratio for all three absorptions was 1.0286 and the 12-32/12-34 ratio was 1.0081, which are nearly the same as those found for CS and suggest a C−S stretching vibration. The constant isotopic frequency ratios and increase on visible (not shown) and ultraviolet photolysis and decrease upon annealing for the three sub-bands supports an assignment of different matrix sites for the same product, as previously shown elsewhere.[26]

It is important to note that the two different carbon−sulfur stretching modes displayed different behaviors upon irradiation and annealing. Upon photolysis, the higher frequency C═S stretching band decreased in intensity, whereas the lower frequency C−S band increased. Upon annealing, the higher frequency C═S stretching absorption increased at the expense of the lower frequency peaks.

Three additional product absorptions were observed at 544.6, 539.0, and 535.2 cm^{-1}. These bands shifted to 535.2, 538.7, and 544.2 cm^{-1} with $^{13}C^{32}S_2$ and to 525.9, 530.0, and 535.2 with $^{12}C^{34}S_2$. The large ^{34}S isotopic shift is indicative of a high sulfur character mode. The peak at 535.2 cm^{-1} decreased intensity upon photolysis and increased intensity upon annealing. This behavior was identical to that of the higher frequency C═S stretching vibration. The bands at 539.0 and 544.6 cm^{-1} increased with photolysis and decreased with annealing, mirroring the behavior of the lower frequency C−S stretching bands. The tracking observed in these two cases demonstrates the presence of two distinct products.

By comparing observed and calculated vibrational frequencies, along with isotopic ratios, two assignments can be made.

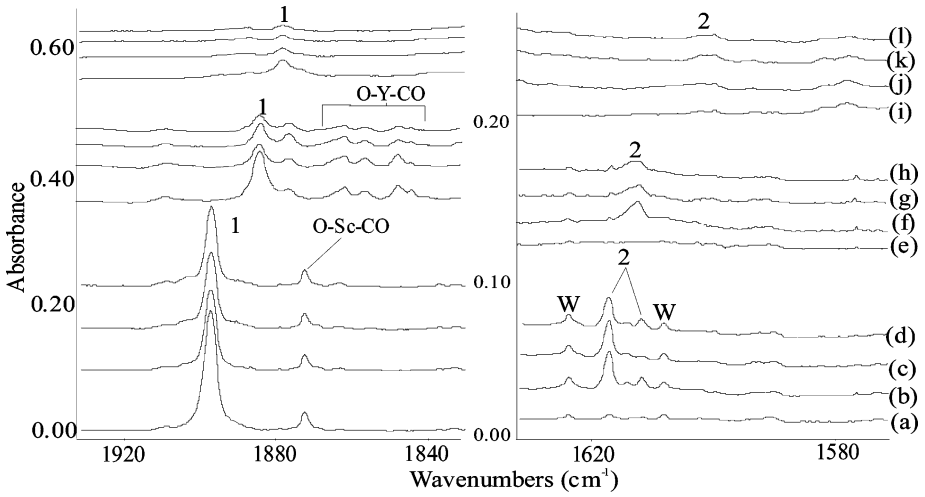

Figure 4. IR spectra in the 1920−1840 and 1620−1580 cm^{-1} regions for group 3 metals and OCS: (a) after 30 min ablation of Sc co-deposited with 0.5% OCS at 8 K in an argon matrix, (b) after 10 min of mercury arc lamp irradiation $\lambda > 290$ nm, (c) after annealing to 25 K, and (d) after 10 min broadband ($\lambda > 220$ nm) irradiation; (e) deposition of Y with 0.5% OCS, (f) $\lambda > 290$ nm irradiation of Y + OCS, (g) after annealing to 25 K, and (h) after 10 min broadband ($\lambda > 220$ nm) irradiation; (i) deposition of La with 0.5% OCS, (j) $\lambda > 290$ nm irradiation of La + OCS, (k) after annealing to 25 K, and (l) after 10 min broadband ($\lambda > 220$ nm) irradiation. Labels 1 and 2 refer to the SMCO and SM(η^2-CO) products, respectively. W denotes water impurity.

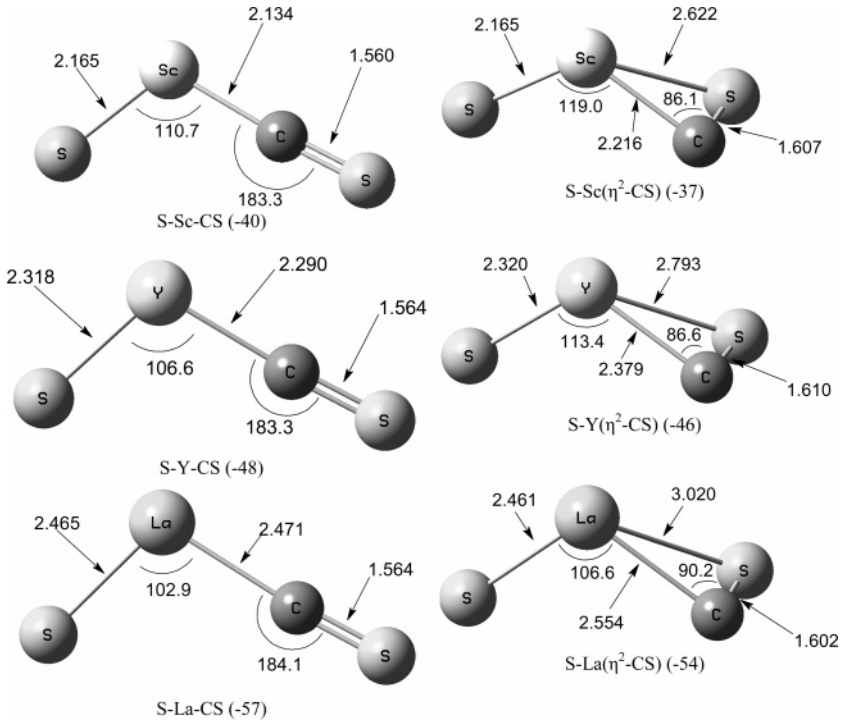

Figure 5. Calculated B3LYP structures (angstroms and degrees) and energies (kcal/mol) relative to M + CS_2 for the group 3 SMCS and SM(η^2-CS) products.

The high-frequency C═S stretching mode (1270.8 cm^{-1}) and the low Sc−S vibration (535.2 cm^{-1}) agree well with the calculated values for a S−Sc−CS type product. Furthermore, the lower C−S stretching peaks (1042.3, 1035.4, and 1027.7 cm^{-1}) and higher Sc−S stretches (539.0 and 544.6 cm^{-1}) are consistent with our calculated S−Sc(η^2-CS) isomer. Values for both calculated and observed products are detailed in Table 1.

Y + CS_2. The results of the Y + CS_2 experiments were similar to the Sc + CS_2 finding. Product absorptions were observed at 1231.6, 1227.4, 1224.0, 1199.3, and 1190.2 cm^{-1}, and 1186.4 cm^{-1}, which shifted to 1201.1, 1194.2, 1188.8, 1185.7, 1161.5, 1152.5, and 1148.9 cm^{-1} with $^{13}C^{32}S_2$ and to 1223.8, 1219.6, 1216.6, 1193.4, 1183.8, and 1180.3 cm^{-1} with $^{12}C^{34}S_2$. The 12-32/13-32 isotopic frequency ratio of 1.0313 and 12-32/12-34 ratio of 1.0064 are in the range for a C═S stretch, but the mode mixing is changing with the metal. Another product band at 1038.0 cm^{-1} was observed to shift to 1029.6 cm^{-1} with $^{13}C^{32}S_2$ and to 1008.9 cm^{-1} with $^{12}C^{34}S_2$. The 12-32/13-32 frequency ratio of 1.0288 and a 12-32/12-34 ratio of 1.0082 are again close to those for CS itself. As in the Sc experiments, the higher frequency C═S stretching mode decreased upon photolysis and increased upon annealing, while the lower frequency C−S stretching mode increased upon photolysis and decreased upon annealing, but smaller relative changes were observed in the Y system. The almost identical behavior of the C═S stretching absorptions during irradiation and annealing characterizes matrix site splitting, as seen with scandium and CS_2. Due to the two distinct behaviors of these bands, the higher frequency modes

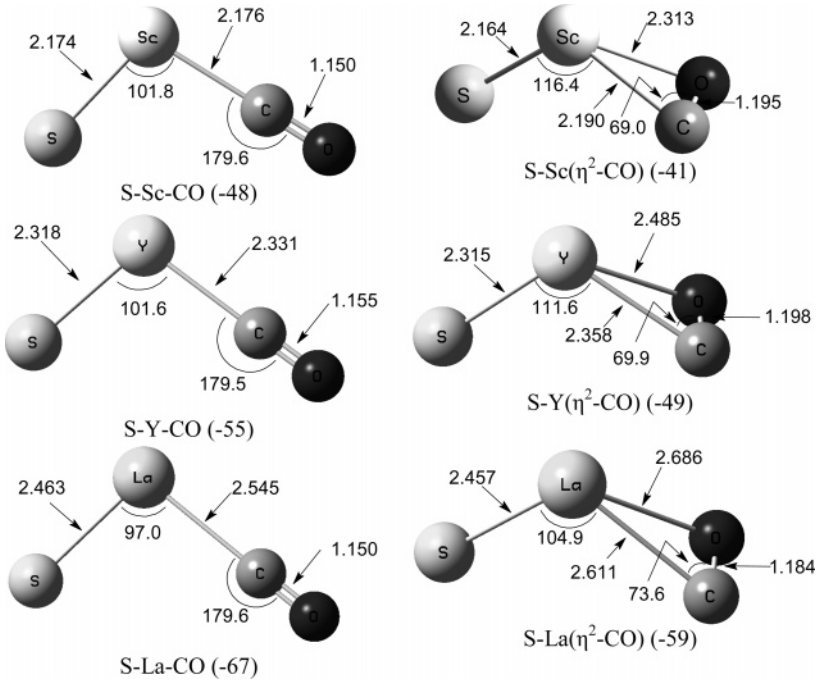

Figure 6. Calculated B3LYP structures (angstroms and degrees) and energies (kcal/mol) relative to M + OCS for the group 3 SMCO and SM-(η^2-CO) products.

are assigned to the S−Y−CS molecule, while the lower frequency stretch is attributed to a S−Y(η^2-CS) type adduct.

One broad band was observed in the Y−S stretching region in these experiments, despite prediction of a Y−S stretch for each of the two products. Additionally, the behavior of the peak was not definitively that of either major assigned product. Fortunately however, two factors support the presence of both isomers: the predicted frequencies were almost identical (469.8 cm^{-1} for S−Y−CS and 469.6 cm^{-1} for S−Y(η^2-CS) at the B3LYP level). Moreover, as mentioned above, in the upper regions of the spectra, the presence of two different carbon−sulfur stretching regions is evidence for both products. Consequently, it is concluded that the two products are superimposed in this region and that the insertion product dominates the spectrum.

La + CS_2. The lanthanum and CS_2 reactions resulted in cleaner spectra than scandium and yttrium. Only one product band was seen in the C═S stretching region. The product absorption at 1206.4 cm^{-1} shifted to 1168.1 cm^{-1} with $^{13}C^{32}S_2$ and to 1200.5 cm^{-1} with $^{12}C^{34}S_2$. The 12-32/13-32 frequency ratio of 1.0328 and a 12-32/12-34 ratio of 1.0049 describe more carbon and less sulfur character for this mostly C═S stretching mode, which is developing antisymmetric M−C−S stretching character. A second C−S stretch was observed at 1044.6 cm^{-1}, which shifted to 1015.6 cm^{-1} with $^{13}C^{32}S_2$ and to 1036.7 cm^{-1} with $^{12}C^{34}S_2$. The 12-32/13-32 ratio of 1.0286 and 12-32/12-34 ratio of 1.0076 are near the ratios for CS itself and confirm the C−S stretching assignment. Low signal-to-noise in the La−S stretching region presented ill-defined peaks, which again combined into one broad absorption for both products, but we believe the insertion product dominates here. The product band was observed at approximately 428 cm^{-1}, and a 10 cm^{-1} shift was observed with $^{12}C^{34}S_2$. No distinguishable $^{13}C^{32}S_2$ shift was detected. As in the scandium and yttrium cases, the higher frequency C═S stretch is attributed to the S−La−CS molecule, while the lower frequency C−S stretch is assigned to S−La-(η^2-CS).

Sc + OCS. Experiments with scandium and natural isotopic carbonyl sulfide resulted in product peaks at 1898.2, 1616.9, 1611.5, and 544.0 cm^{-1}. The band at 1898.2 cm^{-1} was the most intense upon deposition and decreased drastically during photolysis. Little effect was seen during annealing. Peaks at 1616.9, 1611.5, and 544.0 cm^{-1}, although present upon deposition, increased considerably upon photolysis. Annealing produced a decrease in intensity. The close proximity of 1616.9 and 1611.5 cm^{-1} and their identical behavior suggest matrix site splitting, as found in the CS_2 experiments. Consequently, there is evidence for two distinct products in this experiment.

Calculations were performed for many possible scandium reaction products. The Sc(η^2-OC)S, Sc(η^2-SC)O, and Sc(η^3-OCS) association products were not considered for energetic reasons discussed previously. The same argument can be used to discount the CO insertion products: CS insertion remains approximately 20 kcal/mol more favorable than CO insertion according to relative energy calculations. Therefore, only the CS insertion products S−Sc−CO and S−Sc(η^2-CO) are likely to be formed.

Calculated frequencies for S−Sc−CO predicted a CO stretching mode at 2004.4 cm^{-1} with B3LYP and 1925.9 cm^{-1} with the BPW91 method. Therefore, the product peak at 1898.2 cm^{-1} is assigned to this S−Sc−CO carbonyl stretching frequency. In the CS_2 and CO_2 experiments, a X−Sc(η^2-CX) (X = O or S) type product was observed. Moreover, Sc + CO_2 produced O−Sc(η^2-CO) with a CO stretching frequency of 1613.9 cm^{-1}.[17] Calculations predicted CO stretching frequencies for S−Sc(η^2-CO) of 1697.7 cm^{-1} with B3LYP and 1656.1 cm^{-1} with BPW91. These factors suggest that the bands at 1616.9 and 1611.5 cm^{-1} belong to S−Sc(η^2-CO). Additionally, for this product, calculations predict Sc−S stretching frequencies at 559.9 and 545.0 cm^{-1} with B3LYP and BPW91 methods, respectively. This agrees well with the observed peak at 544.0 cm^{-1} and further confirms the presence of S−Sc(η^2-CO). Although S−Sc−CO also possesses a Sc−S stretch, the calculated relative intensities indicate that the Sc−S stretch of S−Sc-(η^2-CO) would be more intense.

Y + OCS. Yttrium reactions with OCS produced bands at 1883.9, 1876.2, 1861.5, 1856.1, 1847.6, 1611.8, and 464.2 cm^{-1}. The bands at 1883.9 and 1876.2 cm^{-1} behave similarly,

decreasing during photolysis, while having the largest intensity upon deposition and annealing. Peaks at 1861.5 and 1856.1 cm^{-1} have been previously reported as the CO stretch of O−Y−CO.[17] Due to comparable behavior, the band at 1847.6 cm^{-1} is probably a matrix site splitting of the CO_2 impurity insertion product. The peaks at 1611.8 and 464.2 cm^{-1} both increase during photolysis. On the basis of this contrasting behavior, two distinct products are formed. Following the above energy arguments, products of the type S−Y−CO and S−Y(η^2-CO) were most likely. The annealing behavior of the bands at 1883.9 and 1876.2 cm^{-1} indicates a high stability product. S−Y−CO was found to be most stable and had calculated frequencies of 1977.7 cm^{-1} (B3LYP) and 2000.7 cm^{-1} (BPW91). Therefore, these two matrix sites can be assigned to the CO stretch of the S−Y−CO product. The calculated lower frequency peak for this product was predicted to be of low intensity and below our experimentally observable region (468.2 and 461.5 cm^{-1} with B3LYP and BPW91, respectively). The CO stretch of O−Y(η^2-CO) has been cited at 1614.5 cm^{-1} in previous work.[17] Calculations predict a CO vibrational frequency of 1681.1 cm^{-1} with B3LYP and 1639.1 cm^{-1} with BPW91. For these reasons, the 1611.8 cm^{-1} band is assigned to the CO stretch of S−Y(η^2-CO). The peak at 464.2 cm^{-1} has the same behavior and compares favorably with the calculated Y−S stretching frequency of 474.4 cm^{-1} with B3LYP and 468.0 cm^{-1} with BPW91. This provides further evidence for the S−Y(η^2-CO) assignment.

La + OCS. Experiments with lanthanum and OCS produced similar products to those found with scandium and yttrium. Product peaks were observed at 1879.0 and 1600.7 cm^{-1}. Calculations for the CO stretch of S−La−CO resulted in 1984.3 cm^{-1} with B3LYP and 1918.0 cm^{-1} with BPW91. Although no O−La−CO matrix study was available, we have already established this region as the CO stretching region for S−M−CO and O−M−CO type molecules. Therefore, the peak at 1879.0 cm^{-1} can be assigned to the CO stretch of S−La−CO. Calculations for the S−La(η^2-CO) product revealed CO stretching frequencies of 1741.1 and 1693.1 cm^{-1} with the B3LYP and BPW91 methods, respectively. Moreover, the above evidence shows that this region contains CO stretching modes of S−M(η^2-CO) and O-M(η^2-CO) molecules. It should be noted that the La−S stretches of both S−La−CO and S−La(η^2-CO) are predicted to fall below our limits of detection: for S−La−CO at 421.0 and 416.0 cm^{-1} with B3LYP and BPW91, respectively; for S−La(η^2-CO) at 427.3 and 422.7 cm^{-1} with B3LYP and BPW91, respectively.

Photoisomerization. Despite the lack of CO insertion, both OCS and CS_2 group 3 reactions formed similar products. Both systems produced an insertion product (S−M−CS and S−M−CO) and a S−M(η^2-CO) or S−M(η^2-CS) side-bound isomer. The behavior of both systems upon annealing and photolysis, coupled with the lack of additional products in the spectra, indicates an interconversion via photolysis and annealing. Upon deposition and annealing, the higher stability adduct S−M−CX is formed (or reformed). Photolysis ($\lambda > 470$ nm and $\lambda > 290$ nm) reduces the intensity of the S−M−CX peaks and increases those of S−M(η^2-CX). As the relative energies of S−M(η^2-CX) products are no more than 10 kcal/mol higher for both OCS and CS_2 systems, isomerization by visible and ultraviolet photolysis is straightforward. Upon annealing to soften the matrix cage, the molecule rearranges back to its most stable form, increasing the intensity of the primary insertion product peaks, as given below (X = O, S).

$$\text{S−M−CX} \underset{\text{Annealing} < 30\ \text{K}}{\overset{\lambda > 290\ \text{nm}}{\rightleftharpoons}} \text{S−M}(\eta^2\text{-CX})$$

A reversible photochemical rearrangement has been reported for the analogous Sc + CO_2 reaction products.[17] Both O−Sc−CO and O−Sc(η^2-CO) type products were characterized. The insertion product increased upon initial annealing and ultraviolet irradiation, and the η^2-CO product increased upon visible photolysis. In this case, the O−Sc(η^2-CO) complex was found to be about 5 kcal/mol higher in energy than O−Sc−CO.

Group Trends. Group trends in both group 3 experiments with CS_2 and OCS were as expected. Vibrational frequencies decreased with increasing metal atomic number for all modes of all molecules. The C═S mode mixing in the SMCS molecules showed more carbon character in a more antisymmetric M−C−S type of motion with increasing metal mass. Furthermore, the isotopic frequency ratios define the vibrational mechanics in this series and verify the SMCS structure and assignments. Calculated geometries for SMCS, SMCO, S−M(η^2-CS), and S−M(η^2-CS) also revealed trends: Bond angles of the type S−M−C decreased with increasing metal atom size. However, M−C−S (or M−C−O) angles of the S−M(η^2-CS) or S−M(η^2-CO) molecules were observed to do the reverse, increasing with atomic size. The M−C−S angle did not change appreciably between the different SMCS and SMCO insertion products. In all products, bond lengths involving the metal atoms increased with the radii of those atoms, as expected. Interestingly, the CS and CO subunits did not differ appreciably in bond length in the different metal systems.

Comparison to the CO_2 System and Previous CS_2 System. As previously mentioned, CS_2 has been studied only once with transition metals.[26] In the late transition metal case, products were of the types SMCS, M−CS_2, and M−(η^2-CS)S. An S−M(η^2-CS) adduct was not observed. This difference could also be attributed to the electron-deficient nature of the group 3 atoms compared with later transition metals. The electron-deficient group 3 metal atoms are satisfied by conversion to an η^2 bridge-type interaction with the CS bond. Late transitions metals have less need for such an effect, and therefore, the S−M(η^2-CS) structure is unfavorable.

Carbon dioxide has also been studied at length with transition metals.[3−14] In experiments with CO_2 and Sc, both OScCO and O−Sc(η^2-CO) adducts were observed.[17] However, with late transition metals (Cr, Mn, Fe, Co, Ni), the bridge-bonded O−M(η^2-CO) complex was not observed.[18] This is a good indication of the metal-dependent energy difference between the two products, which arises because of the electron-deficient nature of Sc and the propensity to form bridge bonds. Additionally, the previous Sc result[17] further supports the present assignments. Finally, as mentioned above, reactions of group 3 transition metals with OCS, CO_2, and CS_2 create two interconvertible isomeric reaction products. This effect was not found in other transition metals with CO_2 and CS_2 systems.

Conclusions

Laser-ablated scandium, yttrium, and lanthanum atoms were co-deposited with CS_2 and OCS in an argon atmosphere. Both SMCX and S−M(η^2-CX) (X = S or O) isomeric products were created upon ablation. These two structural isomers were interconverted upon photolysis and annealing. This is similar to the photochemical reversibility of two analogous S_4 structural isomers.[33,34] The identifications of the products were verified by isotopic substitution and density-functional vibrational frequency and structure calculations.

Acknowledgment. Acknowledgment is made to the Donors of the American Chemical Society Petroleum Research Fund for support of this research.

References and Notes

(1) Pandey, K. K. *Coord. Chem. Rev.* **1995**, *140*, 37.
(2) Peters, J. W. *Science* **2002**, *298*, 552.
(3) Compton, R. N.; Reinhardt, P. W.; Coper, C. D. *J. Chem. Phys.* **1975**, *63*, 3821.
(4) Caballol, R.; Sanchez Marcos, E.; Barthelat, J. C. *J. Phys. Chem.* **1987**, *91*, 1328.
(5) Jeung, G. H. *Mol. Phys.* **1989**, *67*, 747.
(6) Lessen, D. E.; Asher, R. L.; Brucat, P. J. *J. Chem. Phys.* **1991**, *95*, 1414.
(7) Schwarz, J.; Schwarz, H. *Organometallics* **1994**, *13*, 1518.
(8) Asher, R. L.; Bellert, D.; Buthelezi, T.; Weerasekera, G.; Brucat, P. J. *Chem. Phys. Lett.* **1994**, *228*, 390.
(9) Sodupe, M.; Branchadell, V.; Oliva, A. *J. Phys. Chem.* **1995**, *99*, 8567.
(10) Galan, F.; Fouassier, M.; Tranquille, M.; Mascetti, J.; Papai, I. *J. Phys. Chem. A* **1997**, *101*, 2626.
(11) Papai, I.; Mascetti, J.; Fournier, R. *J. Phys. Chem. A* **1997**, *101*, 4465.
(12) Fan, H. J.; Liu, C. W. *Chem. Phys. Lett.* **1999**, *300*, 351.
(13) Xu, Q.; Jiang, L. *J. Phys. Chem. A* **2006**, *110*, 2655.
(14) Sievers, M. R.; Armentrout, P. B. *J. Chem. Phys.* **1995**, *102*, 754.
(15) Papai, I. *Book of Abstracts*; 213th ACS National Meeting, San Francisco, CA, April 13−17, 1997; COMP.
(16) Zhou, M.; Andrews, L. *J. Phys. Chem. A* **1999**, *103*, 2066.
(17) Zhou, M.; Andrews, L. *J. Am. Chem. Soc.* **1998**, *120*, 13230.
(18) Zhou, M.; Liang, B.; Andrews, L. *J. Phys. Chem. A* **1999**, *103*, 2013.
(19) Walker, N. R.; Walters, R. S.; Grieves, G. A.; Duncan, M. A. *J. Chem. Phys.* **2004**, *121*, 10498.
(20) Zhang, X. G.; Armentrout, P. B. *J. Phys. Chem. A* **2003**, *107*, 8904.
(21) Li, T.; Xie, X.; Gao, S.; Wang, C.; Cheng, W.; Pan, X.; Cao, H. *THEOCHEM* **2005**, *724*, 125.
(22) Gao, L.-G.; Wang, Y.-C.; Geng, Z.-Y.; Chen, X.-X.; Lu, L.-L.; Dai, G.-L.; Wang, D.-M. *Wuli Huaxue Xuebao* **2005**, *21*, 1102.
(23) Dobrogorskaya, Y.; Mascetti, J.; Papai, I.; Nemukhin, A.; Hannachi, Y. *J. Phys. Chem. A* **2003**, *107*, 2711.
(24) Huber, H.; Ozin, G. A.; Power, W. J. *Inorg. Chem.* **1977**, *16*, 2234.
(25) Rue, C.; Armentrout, P. B.; Kretzschmar, I.; Schroder, D.; Harvey, J. N.; Schwarz, H. *J. Chem. Phys.* **1999**, *110*, 7858.
(26) Zhou, M. F.; Andrews, L. *J. Phys. Chem. A* **2000**, *104*, 4394.
(27) Rue, C.; Armentrout, P. B.; Kretzschmar, I.; Schroder, D.; Schwarz, H. *Int. J. Mass Spectrosc.* **2001**, *210/211*, 283.
(28) Rue, C.; Armentrout, P. B.; Kretzschmar, I.; Schroeder, D.; Schwarz, H. *J. Phys. Chem. A* **2001**, *105*, 8456.
(29) Rue, C.; Armentrout, P. B.; Kretzschmar, I.; Schroeder, D.; Schwarz, H. *J. Phys. Chem. A* **2002**, *106*, 9788.
(30) Jiang, N.; Zhang, D. *Chem. Phys. Lett.* **2002**, *366*, 253.
(31) Cheng, P.; Koyanagi, G. K.; Bohme, D. K. *J. Phys. Chem. A* **2006**, *110*, 2718.
(32) Kretzschmar, I.; Schroder, D.; Schwarz, H.; Armentrout, P. B. *Int. J. Mass Spectrosc.* **2006**, *249*, 263.
(33) Hassanzadeh, P.; Andrews, L. *J. Phys. Chem.* **1992**, *96*, 6579.
(34) Brabson, G. D.; Mielke, Z.; Andrews, L. *J. Phys. Chem.* **1991**, *95*, 79.
(35) Burkholder, T. R.; Andrews, L. *J. Chem. Phys.* **1991**, *95*, 8697.
(36) Hassanzadeh, P.; Andrews, L. *J. Phys. Chem.* **1992**, *96*, 9177.
(37) Zhou, M.; Andrews, L. *J. Chem. Phys.* **1999**, *110*, 10370.
(38) Frisch, M. J.; Trucks, G. W.; Schlegel, H. B.; Scuseria, G. E.; Robb, M. A.; Cheeseman, J. R.; Zakrzewski, V. G.; Montgomery, J. A., Jr.; Stratmann, R. E.; Burant, J. C.; Dapprich, S.; Millam, J. M.; Daniels, A. D.; Kudin, K. N.; Strain, M. C.; Farkas, O.; Tomasi, J.; Barone, V.; Cossi, M.; Cammi, R.; Mennucci, B.; Pomelli, C.; Adamo, C.; Clifford, S.; Ochterski, J.; Petersson, G. A.; Ayala, P. Y.; Cui, Q.; Morokuma, K.; Rega, N.; Salvador, P.; Dannenberg, J. J.; D. K. Malick; Rabuck, A. D.; Raghavachari, K.; Foresman, J. B.; Cioslowski, J.; Ortiz, J. V.; Baboul, A. G.; Stefanov, B. B.; Liu, G.; Liashenko, A.; Piskorz, P.; Komaromi, I.; Gomperts, R.; Martin, R. L.; Fox, D. J.; Keith, T.; Al-Laham, M. A.; Peng, C. Y.; Nanayakkara, A.; Challacombe, M.; Gill, P. M. W.; Johnson, B.; Chen, W.; Wong, M. W.; Andres, J. L.; Gonzalez, C.; Head-Gordon, M.; Replogle, E. S.; Pople, J. A. *Gaussian 98*, revision A.11.4; Gaussian, Inc.: Pittsburgh, PA, 2002.
(39) Becke, A. D. *J. Chem. Phys.* **1993**, *98*, 5648.
(40) Lee, C. T.; Yang, W. T.; Parr, R. G. *Phys. Rev. B* **1988**, *37*, 785.
(41) Becke, A. D. *Phys. Rev. A* **1988**, *38*, 3098.
(42) Perdew, J. P.; Wang, Y. *Phys. Rev. B* **1992**, *45*, 13244.
(43) Krishnan, F.; Binkley, J. S.; Seeger, R.; Pople, J. A. *J. Chem. Phys.* **1980**, *72*, 650.
(44) Frisch, M. J.; Pople, J. A.; Binkley, J. S. *J. Chem. Phys.* **1984**, *80*, 3265.
(45) Andrae, D.; Haussermann, U.; Dolg, M.; Stoll, H.; Preuss, H. *Theor. Chim. Acta* **1990**, *77*, 123.
(46) Zhou, M.; Andrews, L. *J. Chem. Phys.* **2000**, *112*, 6576.
(47) Chertihin, G. V.; Andrews, L.; Rosi, M.; Bauschlicher, C. W. *J. Phys. Chem. A* **1997**, *101*, 9085.
(48) Andrews, L.; Zhou, M. F.; Chertihin, G. V.; Bauschlicher, C. W. *J. Phys. Chem. A* **1999**, *103*, 6525.
(49) Papai, I.; Hannachi, Y.; Gwizdala, S.; Mascetti, J. *J. Phys. Chem. A* **2002**, *106*, 4181.